

Rare Earth Doped Metal Oxide Sensors for the Detection of Methane at Room Temperature

José P. Santos*, Carlos Sanchez-Vicente, Isabel Sayago

Nanosensors and Intelligent System Group, NOySI (ITEFI, CSIC). Madrid, Spain.
jp.santos@csic.es

This work describes the behavior of a matrix of nanosensors based on metal oxides (MOS) for detecting of methane and carbon dioxide (greenhouse gases) at room temperature. The materials used were tin oxide and zinc oxide nanoparticles. The sensors were deposited via dropcasting from aqueous solutions of MOS nanoparticles. Some of the sensors were doped with terbium to evaluate their catalytic properties, and to leverage their optical properties, exploring the possibility of an opto-resistive sensor. Measurements of both gases were taken at different concentrations and at 50% relative humidity to simulate real-world conditions as closely as possible.

During the measurement process, the nanosensor matrix was illuminated with an ultraviolet lamp for two purposes: to promote gas adsorption and desorption on the material surface, achieving a quicker electrical response, and to excite the material with ultraviolet light to collect the subsequent photoluminescence (PL) emitted by it and observe the change that occurs in the presence of the target gases.

The results demonstrate that the sensors are capable of detecting both compounds, as there is a resistive variation when the sensor is exposed to these gases. However, there is no variation in the photoluminescence emitted by the material when excited with an ultraviolet lamp in the presence of methane.

1. Introduction

Air quality control is a matter of great concern due to its impact on the environment and health. Consequently, there is an urgent demand for toxic gas detection. Methane (CH₄) is a greenhouse gas (GHG) that, in addition to exacerbating the climate crisis, degrades air quality and thus human health. It has 80 times the warming potency of carbon dioxide (CO₂) over a 20-year period. Methane emissions account for nearly 25% of global warming (IEA, 2022). Methane also affects air quality by contributing to ground level (tropospheric) ozone, a dangerous pollutant. Current concentration of methane is about 1.92 ppm.

Over the past decades, metal oxide semiconductors (MOS) have been considered the most powerful materials for gas detection (Yamazoe et al., 2003 and Inoue et al., 1995). However, the detection properties of MOS-based gas sensors need improvement in terms of sensitivity, selectivity, stability, energy consumption, and cost. To this end, nanotechnology is driving the research of new advanced materials such as thin films (Sberveglieri, 1995), nanobelts (Comini et al., 2002), nanowires (Zhang D. et al., 2004), and nanofibers (Kim et al., 2006), which have been used to enhance detection performance.

Thin films made of nanoparticles (NPs) are characterized by a high surface area relative to their volume. The arrangement of these nanoparticles generates surface porosity, which in turn increases the material's surface area. These films can be easily fabricated using techniques like dropcasting, an economical and rapid method for depositing materials onto substrates. In previous research, sensors fabricated using this technique with different metal oxides have been electrically characterized by measuring the variation in electrical resistance. This work introduces the novelty of characterizing the material using optical techniques in conjunction with electrical measurements. This involves doping the metal oxide with rare earth elements, which exhibit photoluminescent properties when illuminated with ultraviolet light. The response of these materials to exposure to greenhouse gases such as methane and CO₂ has been evaluated using both characterization methods,

aiming to obtain more comprehensive information from each measurement. This approach allows for complementary information, improving the selectivity of these sensors.

2. Experimental

2.1 Materials

Tin oxide (SnO_2) and zinc oxide (ZnO) nanoparticles have been used as the main materials. Additionally, terbium (Tb) has been used as a dopant (in powder form, and soluble in water). Dispersions of the materials were prepared in deionized water at a ratio of 2.5 mg/mL. Furthermore, Tb was present in a 10% w/w proportion. The dispersions were sonicated for 10 minutes before being deposited onto the substrates. Table 1 shows the composition of the different dispersions made for each of the nanosensors and the sizes of nanoparticles used in each case.

Table 1: Sensors dispersions of nanoparticles

Sensor	Material	MOS NP diameter (nm)
S1	SnO_2	100
S2	ZnO	50
S3	$\text{SnO}_2 + \text{Tb}$	100
S4	$\text{ZnO} + \text{Tb}$	50

The multi-sensor platform (Figure 1) used includes 4 membranes that can be functionalized with different materials. It is made of FR-4 (Eurocircuits NV, Belgium), with dimensions of 15.24 mm in diameter and 0.3 mm in thickness. It is flame resistant, has nearly zero water absorption, and a wide operating temperature range (from 50°C to 115°C). However, in this case, measurements are taken at room temperature.

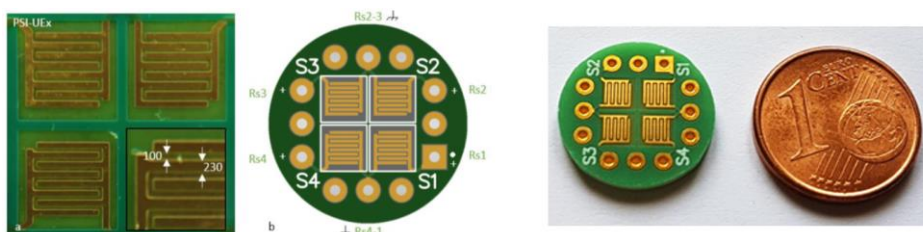


Figure 1: Multisensory platform

2.2 Devices

For the manufacturing of the different sensitive layers deposited on the membranes of the multi-sensor platform, a homemade device called a drop-caster was used. This device, described in previous works (Santos et al., 2021), automates the dropcasting process. The device is shown in Figure 2.

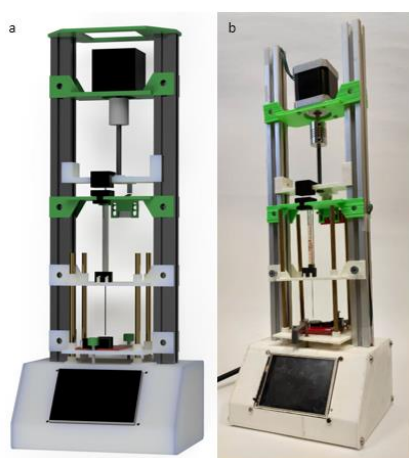


Figure 2: Dropcaster. (a) Rendering of 3D design. (b) Dropcaster fabrication and assembled

In this work, droplets of 90 nL were deposited. Water was used as the solvent for making the dispersions due to its higher surface tension. This allows for more compact droplets and prevents the solvent from spreading over the membrane surface, resulting in a reduced deposition area. During the deposition process, the sensor surface was illuminated with an infrared lamp to promote the solvent's evaporation and expedite the process.

2.3 Morphological characterization

Different morphological characterizations have been performed to observe the behavior of the nanoparticles (NPs) and the deposition process. The sensitive films were morphologically characterized by scanning electron microscopy (SEM, Quanta 3D FEG, FEI, Hillsboro, OR, USA) and transmission electron microscopy (TEM, JEOL JEM 2100). Finally, since this work will combine electrical and optical measurements simultaneously, the material has also been optically characterized to determine its photoluminescence when excited with an argon laser measured with a Digital OR pulse combining photomultiplier.

2.4 Measurement setup

Electrical characterization was carried out using a scanning electrometer (6517, Keithley, Cleveland, OH, USA) at a constant bias voltage of 15 V. The array of nanosensors was illuminated with an ultraviolet LED with a wavelength of 365 nm (LSM-365A Light Source, Ocean Insight, FL, USA). This LED is controlled by a controller that allows modulation of the LED power and generated waveform (LDC-1 Single Channel LED Controller, Ocean Insight, FL, USA). The light emission generated by lamp excitation is collected by a spectrometer (HR2 UV-VIS, Ocean Insight, FL, USA). The transmission of the optical signal from the LED to the measurement cell, and from there to the spectrometer is carried out using optical fibers. Both the LED, the cell, and the spectrometer incorporate SMA connectors to directly connect the fiber to each device.

Measurements of the target gas were conducted at a constant flow rate of 100 mL/min. The analyte exposure time was 15 minutes, followed by a recovery phase was 30 minutes. CO₂ concentrations (100 to 500 ppm) and CH₄ concentrations (2 to 10 ppm) were generated using a gas mixing unit (GMU, Ray IE, Mirabel, Spain) from calibrated bottles (certified by Nippon Gases S.L.U.). The measurements were conducted at room temperature. The generated gas samples were at 50% relative humidity. The measurement process and equipment are controlled using software developed with LabVIEW.

The measurement cell contains a chamber in the middle, where the sensor is housed, with an O-ring for sealing it to the PCB to ensure proper sealing. The electrical signal is collected through this PCB. It includes two fittings to connect it to the GMU using Teflon tubes. Additionally, it incorporates two fittings on the top to connect the emission and reception optical fibers. The UV light emission from the LED is directed at a 45° angle to the sensor surface, while the reception of the reflected signal is carried out at a 90° angle to the sensor surface.

Figure 3 shows the laboratory setup used to prepare the gas mixture and verify the sensors' functionality.

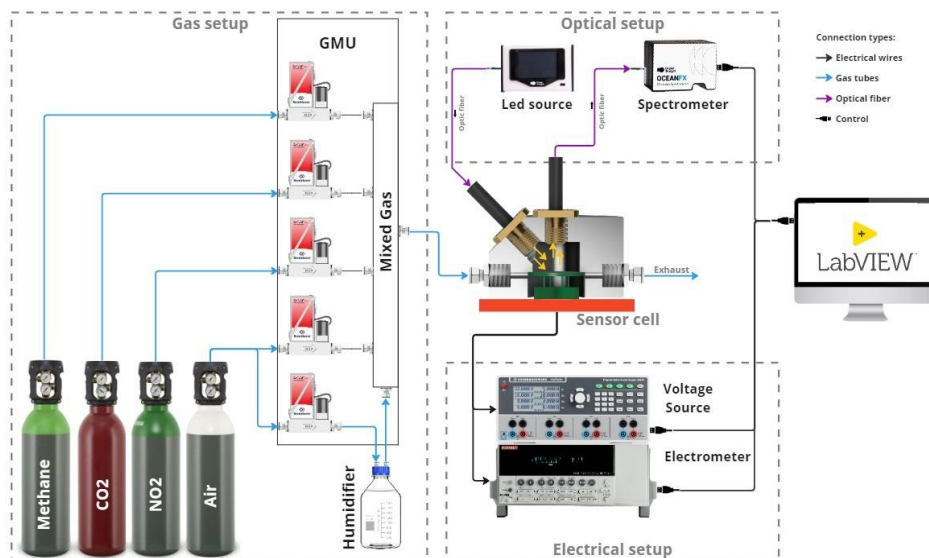


Figure 3: Measurement setup

The response is defined as follows:
$$r (\%) = \frac{R - R_a}{R_a} \times 100 \quad (1)$$

where R is the resistance of the device at the end of exposure to target gas, and R_a is the resistance in air.

3. Results and discussion

3.1 Morphological characterization

In Figure 4, the arrangement of the deposited samples can be observed. A homogeneous distribution of the NPs on the sensor surface is visible, although in certain areas, clusters of NPs can be seen, which may be due to poor dispersion during the deposition process. Additionally, areas with higher porosity can be seen in certain areas, which can be beneficial in increasing the surface area of the deposited material.

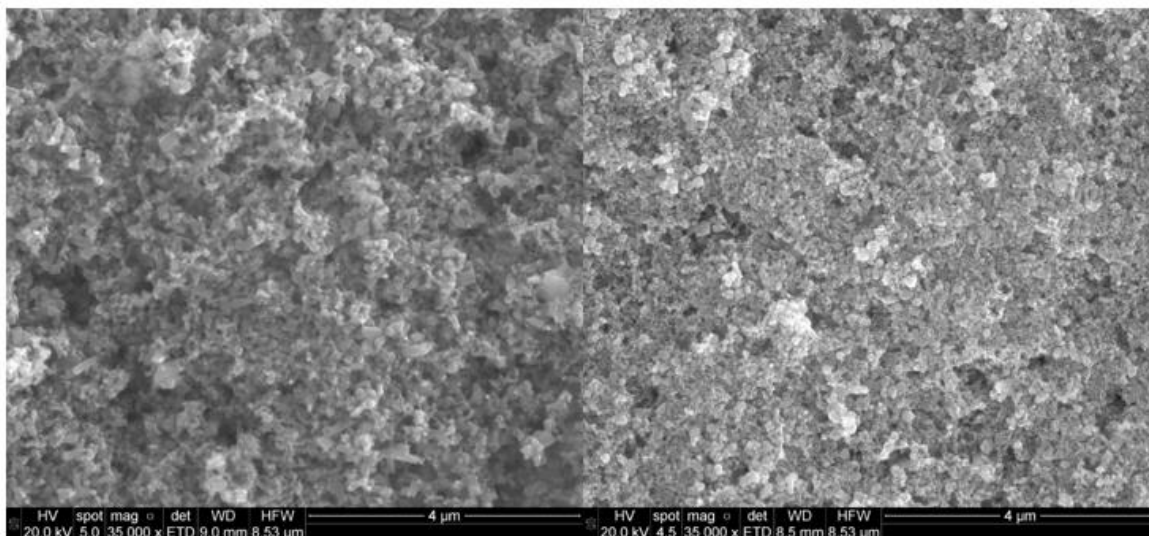


Figure 4: SEM images of SnO₂ (left) and ZnO (right) (images made by University of Extremadura).

On the other hand, the samples were also characterized using TEM to observe in greater detail the number of clusters formed and their size, as shown in Figure 5. Larger clusters can be found, but generally, majority of crystals correspond to the size given by the manufacturer. Since observing a sample with TEM requires depositing a single layer, it can be concluded that the NPs are indeed well dispersed in the solution but agglomerate during the material deposition process, when multiple layers are successively deposited on top of each other. In the spectrum obtained with EDX, the presence of Tb in the deposited material can be observed.

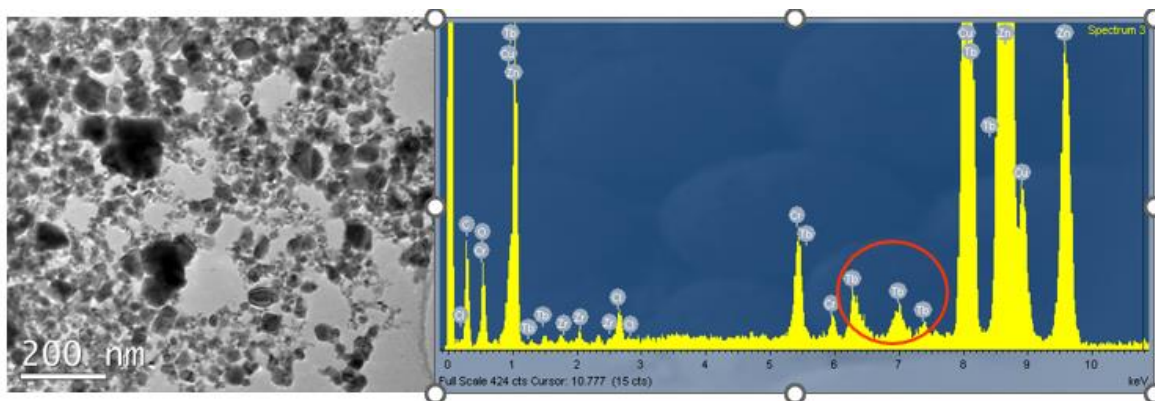


Figure 5: TEM images and EDX spectrum of ZnO + Tb (images made by National Center for Electron Microscopy).

3.2 Electrical characterization

The SnO₂ sensors were shown to be able to detect the different concentrations of CO₂ and CH₄. It should be noted that the Tb-doped sensor has a lower response to the same CO₂ concentrations, but a greater difference is observed between low and medium concentrations, while the undoped sensor responds much more similarly for all concentrations. The ZnO sensors did not respond in the presence of CO₂, but did respond in the presence of CH₄. Figure 6 shows an example of the electrical response of the ZnO sensor in the presence of CH₄; it can

be observed that the sensor recovers quickly after each measurement, with a recovery time consistently around 6 minutes.

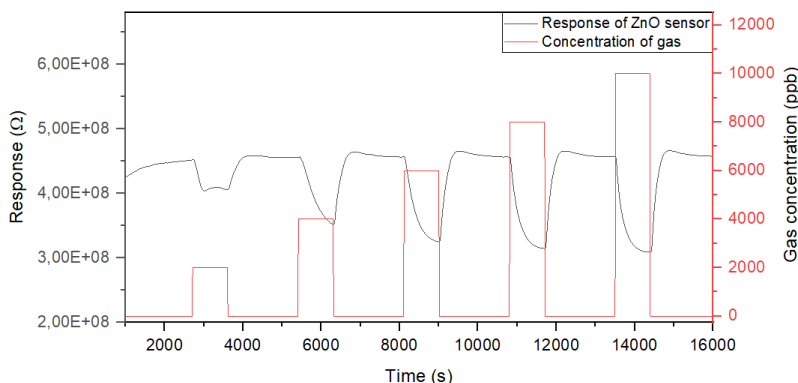


Figure 6: Electrical response of the ZnO sensor in the presence of different concentrations of CH_4 .

The ZnO and SnO₂ sensors responded when exposed to a CH_4 atmosphere. It can be observed in Figure 7 that at higher concentrations, the undoped sensors have a greater response to CH_4 , similar to what happens in experiments conducted with CO_2 . The ZnO + Tb sensor exhibits a lower response to CH_4 , and there is also less difference in response between concentrations of this gas.

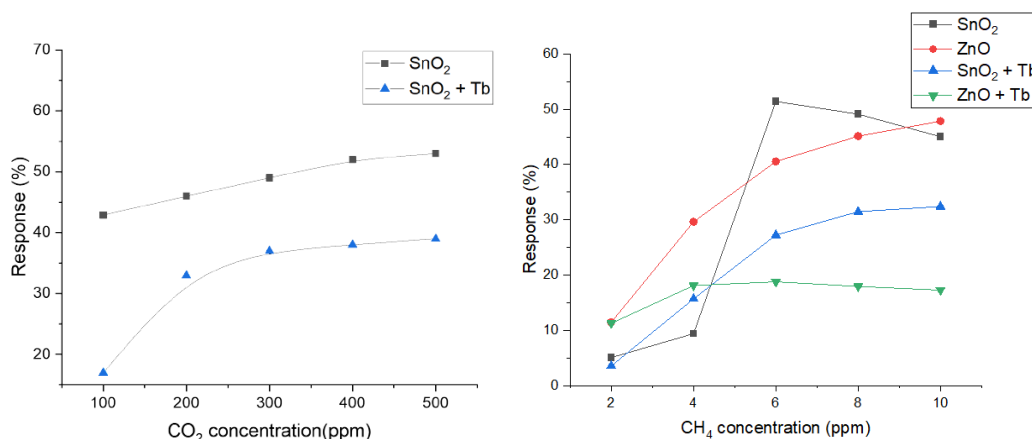


Figure 7: Electrical response of the sensors in the presence of CO_2 and CH_4 at different concentrations.

3.3 Optical Characterization

SnO₂ is an N-type semiconductor with a large band gap ($E_g = 3.6$ eV at 300 K) and oxygen vacancies are identified as the primary defects in SnO₂ and typically act as the radiative centers in PL processes. The PL properties are influenced by the size effects, defects (such as oxygen vacancies) and surface capping. These oxygen vacancies characteristically act as deep defect donors in SnO₂ and would cause the formation of new donor levels in the band gap. Therefore, the PL emission of SnO₂ is attributable to a transition of an electron from a level close to the conduction band edge to a deeply trapped hole in the bulk of the SnO₂ nanocrystals (Periyasamy and Kar, 2020). The same situation occurs with ZnO that has a band gap of 3.37 eV at 300 K. The green emission with 490 nm wavelength may originate from the electron transition from the level of the ionized oxygen vacancies to the valence band (Zhang D.H. et al., 2003).

As mentioned in the previous section, the sensor was exposed to different atmospheres by irradiating it with a UV LED. Figure 8 shows the spectra obtained in the presence of CO_2 and CH_4 . In both cases, the measured wavelengths correspond to values found in the literature. When exposed to CO_2 , a difference in spectrum amplitude is observed compared to when only air is present. Conversely, no noticeable difference is observed in the presence of CH_4 . This could be because CH_4 does not alter the photoluminescent properties of the material. However, it's important to note that the maximum measured concentration of CH_4 is 50 times lower than that of CO_2 .

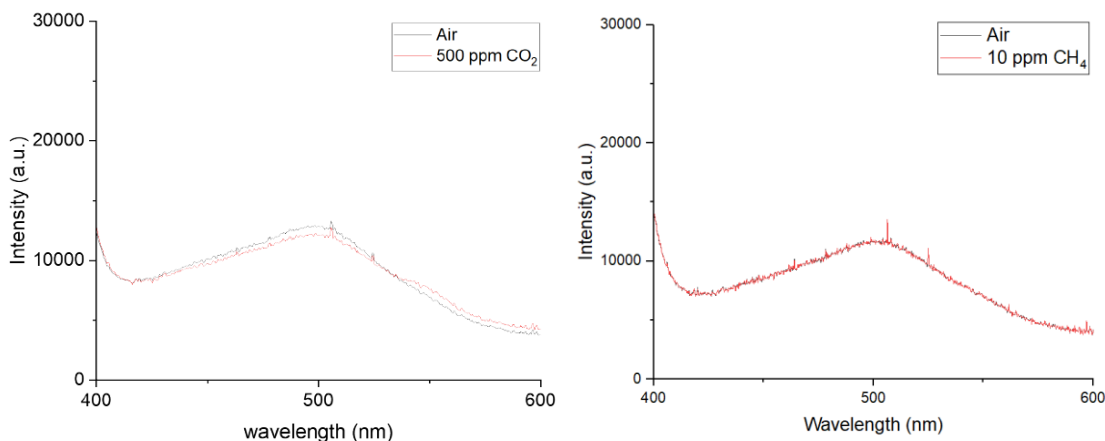


Figure 8: Optical response of the sensors in the presence of CO_2 and CH_4 at different concentrations.

4. Conclusion

In this work, we developed low-cost sensors for the detection of methane and CO_2 based on SnO_2 and ZnO nanoparticles. The sensor performances were evaluated based on their response, response/recovery time to both gases.

The optical properties were analyzed by illuminating the sensors with ultraviolet light. The sensors incorporating SnO_2 showed differences in the optical spectrum in the presence of CO_2 but not in the presence of methane. It's possible that similar differences would be observed with methane at higher concentrations, as the maximum concentration of CO_2 used is 50 times higher than the highest methane concentration.

The use of Tb as a dopant improved the optical properties of the SnO_2 sensor but deteriorated the electrical properties in both SnO_2 and ZnO sensors for both gases. Nevertheless, all sensors were capable of detecting CH_4 , even differentiating between different concentrations of this gas. In contrast, only sensors made with SnO_2 are capable of responding to different CO_2 concentrations, while sensors incorporating ZnO do not respond to this gas. Exploring the use of both materials to distinguish gas mixtures could be intriguing. Future work will involve cross-measurements with these two gases to verify this hypothesis.

References

- Comini E., Faglia G., Sberveglieri G., Pan Z., Wang Z.L., 2002, Stable and highly sensitive gas sensors based on semiconducting oxide nanobelts, *Appl. Phys. Lett.*, 81, 1869–1871.
- Inoue T., Ohtsuka K., Yoshida Y., Matsuura Y., Kajiyama Y., 1995, Metal oxide semiconductor NO_2 sensor, *Sensors Actuators B Chem.* 25, 388–391.
- IEA, 2022, International Energy Agency: IEA <www.iea.org/energy-system/fossil-fuels/methane-abatement> accessed 08.03.2024
- Kim I.-D., Rothschild A., Lee B.H., Kim D.Y., Jo S.M., Tuller H.L., 2006, Ultrasensitive chemiresistors based on electrospun TiO_2 nanofibers, *Nano Lett.*, 6, 2009–2013.
- Periyasamy M., Kar A., 2020, Modulating the properties of SnO_2 nanocrystals: morphological effects on structural, photoluminescence, photocatalytic, electrochemical and gas sensing properties. *J. Mater. Chem. C*, 8, 4604
- Santos J.P., Sánchez-Vicente C., Azabal A., Ruiz-Valdepeñas S., Lozano J., Sayago I., Sanjurjo J.L., 2021, Automation and optimization device for the fabrication of sensors with nanomaterials, 13th Spanish Conference on Electron Devices Proceeding, Sevilla, Spain, 129 – 131
- Sberveglieri G., 1995, Recent developments in semiconducting thin-film gas sensors, *Sensors Actuators B. Chem.* 23, 103–109.
- Yamazoe N., Sakai G., Shimanoe K., 2003, Oxide Semiconductor Gas Sensors, *Catal. Surv. from Asia*, 7, 63–75.
- Zhang D., Liu Z., Li C., Tang T., Liu X., Han S., Lei B., Zhou C., 2004, Detection of NO_2 down to ppb levels using individual and multiple In_2O_3 nanowire devices, *Nano Lett.*, 4, 1919–1924.
- Zhang D.H., Wang Q.P., Xue Z.Y., 2003, Photoluminescence of ZnO films excited with light of different wavelength. *Applied Surface Science*, 207, 20–25.